European Journal of Medicinal Chemistry 316 (2026) 119037

Contents lists available at ScienceDirect

European Journal of Medicinal Chemistry

journal homepage: www.elsevier.com/locate/ejmech

Research paper

First-in-class nonsteroidal anti-inflammatory drug and carbonic anhydrase inhibitor hybrid compounds as effective antimycobacterial agents

Jenny Parkkinen [a,*], Özlem Akgul [b,c], Emanuela Berrino [b], Fabrizio Carta [b,**], Silvia Selleri [b], Milka Hammarén [a], Ashok Aspatwar [a], Gianluca Bartolucci [b], Clemente Capasso [d], Mataleena Parikka [a,1], Seppo Parkkila [a,e,1], Claudiu T. Supuran [b,1]

[a] Faculty of Medicine and Health Technology, Tampere University, Arvo Ylpön katu 34, Tampere, 33520, Finland
[b] NEUROFARBA Department, Sezione di Scienze Farmaceutiche e Nutraceutiche, University of Florence, via Ugo Schiff 6, Sesto Fiorentino, FI, 50019, Italy
[c] Department of Pharmaceutical Chemistry, Faculty of Pharmacy, Ege University, Bornova, İzmir, 35100, Turkey
[d] Department of Biology, Agriculture and Food Sciences, CNR, Institute of Biosciences and Bioresources, Via Pietro Castellino 111, Napoli, 80131, Italy
[e] Department of Clinical Chemistry, Fimlab Laboratories PLC, Arvo Ylpön katu 4, Tampere, 33520, Finland

ARTICLE INFO

Keywords:
Carbonic anhydrase inhibitor
Host-directed therapy
Mycobacterium marinum
Mycobacterium tuberculosis
Nonsteroidal anti-inflammatory drug
Tuberculosis
Zebrafish

ABSTRACT

We investigated the *in vitro* effects of nonsteroidal anti-inflammatory drug-carbonic anhydrase inhibitor hybrids (NSAID-CAIs) on β-carbonic anhydrases 1-3 expressed by *Mycobacterium tuberculosis*, as well as their antimycobacterial efficacy in a zebrafish infection model. The primary aims were to investigate whether these enzymes represent valid therapeutic targets and whether NSAID-CAIs constitute potential drug candidates for tuberculosis. *In vitro* inhibition activity against the carbonic anhydrases was evaluated with a CO_2-hydration assay. Antimycobacterial properties of the NSAID-CAIs were assessed via screening assays based on bioluminescence and colony-forming units. Larval and adult zebrafish were used for *in vivo* experiments. NSAID-CAIs strongly inhibited *Mycobacterium tuberculosis* β-carbonic anhydrase 2 and human carbonic anhydrases IX and XII *in vitro*. They exhibited high efficacy against *Mycobacterium marinum* and attenuated *Mycobacterium tuberculosis* in biofilm environments, outperforming their coadministered constitutive fragments. Compounds **11**, **19**, and **24** showed bactericidal properties against *Mycobacterium marinum,* and **12** was able to potentiate the effects of rifampicin. The experimental data provides solid *in vitro* evidence for the use of NSAID-CAIs as antimycobacterial agents by means of *Mycobacterium tuberculosis* β-carbonic anhydrase inhibition along with the possible suppression of the host immune response through the induction of host-directed therapeutic effects.

1. Introduction

Tuberculosis (TB) caused by *Mycobacterium tuberculosis* (Mtb) remains one of the deadliest infectious diseases worldwide. According to World Health Organization (WHO) reports, more than 10 million annual TB cases were directly linked to 1.25 million deaths in 2023 [1]. Approximately a quarter of the global human population is estimated to carry Mtb, and the associated risk of disease activation ranges between 5% and 10% [2]. The treatment of TB involves combinations of several antimicrobials and typically lasts for several months [2,3]. Promoted by the suboptimal efficacy of the current treatment regime, over 400,000 cases of multidrug-resistant TB (MDR-TB) arise annually, thus emphasizing the high demand for more robust alternative treatments [2,4]. Countries with moderate to high incidences of isoniazid- and rifampicin-resistant TB are recommended to utilize the Bacillus Calmette-Guérin (BCG) vaccine [5]. Among the mechanisms to persist the effects of antimicrobial drugs is the formation of extracellular biofilms, which provide physical cover and enable the growth of tolerant

* Corresponding author.
** Corresponding author.
E-mail addresses: jenny.parkkinen@tuni.fi (J. Parkkinen), ozlem.akgul@ege.edu.tr (Ö. Akgul), emanuela.berrino@gmail.com (E. Berrino), fabrizio.carta@unifi.it (F. Carta), silvia.selleri@unifi.it (S. Selleri), milka.hammaren@tuni.fi (M. Hammarén), ashok.aspatwar@tuni.fi (A. Aspatwar), gianluca.bartolucci@unifi.it (G. Bartolucci), clemente.capasso@ibbr.cnr.it (C. Capasso), mataleena.parikka@tuni.fi (M. Parikka), seppo.parkkila@tuni.fi (S. Parkkila), claudiu.supuran@unifi.it (C.T. Supuran).
[1] Equal contribution as co-senior authors.

https://doi.org/10.1016/j.ejmech.2026.119037
Received 6 March 2026; Received in revised form 20 April 2026; Accepted 3 June 2026
Available online 3 June 2026
0223-5234/© 2026 The Authors. Published by Elsevier Masson SAS. This is an open access article under the CC BY license (http://creativecommons.org/licenses/by/4.0/).

subpopulations [2,3,6]. Biofilms have long been overlooked in the context of Mtb virulence and targeted drug development [2,7]. Another radical change for tackling TB is represented by the host-directed therapy (HDT) approach, which targets the host immune system rather than the etiologic agent itself [8,9]. In TB, Mtb prevents the effective activation of host proinflammatory responses and adopts diverse immune evasion mechanisms [10]. As a result of the hosts' immune responses, Mtb are encapsulated within granulomas that allow the pathogen to survive for decades in a latent state and possibly then reactivate [11]. Granulomas efficiently shield mycobacteria from any xenobiotic, including antimicrobial drugs [11]. The concept of mitigating excessive host inflammatory responses as part of anti-TB strategies has led to the inclusion of host-targeting NSAIDs, with clinical outcomes to date being highly encouraging for further development [8,12]. These results agree with the evidence on commercially available NSAIDs coupled with prototypic inhibitors of human carbonic anhydrases (hCAs; EC 4.2.1.1), such as primary sulfonamides and coumarins [13–17]. Overall, NSAID-CA inhibitors (NSAID-CAIs) showed greater efficacy in attenuating inflammatory responses in inflammation, lung fibrosis, and rheumatoid arthritis *in vivo* models than did the coadministration of their individual NSAID and CAI components. These results were indicative of a potential anti-inflammatory effect mediated by CA inhibition (i.e., tumor- and autoimmune-associated hCA IX and XII) [18]. Interestingly, mycobacterial β-CAs are predicted to be involved in biofilm formation, as the clinically used CAI ethoxzolamide reduces the transport of extracellular DNA (eDNA), a key component of the biofilm matrix [19]. A library of eDNA-deficient mutants listed CAs as relevant hits, thus linking them with biofilm formation processes [19]. Therefore, the possible inhibitory effects of NSAID-CAIs on Mtb β-CAs, combined with the potential HDT effect, may position them as promising candidates for anti-TB therapy.

The first aim of this study was to investigate whether NSAID-CAIs may be effective inhibitors of Mtb β-CA1 (encoded by the Rv1284 gene), β-CA2 (Rv3588c), and β-CA3 (Rv3273) [20–22]. Second, we investigated whether these NSAID-CAIs exhibit antimycobacterial activity that surpasses that achieved by the coadministration of their individual NSAID and CAI components. In addition to their antimycobacterial activity, we aimed to explore the biofilm-interfering properties of the compounds. Specifically, we investigated tolerant mycobacterial subpopulations, which are commonly overlooked in TB preclinical studies, via a minimum duration for killing (MDK) method developed in house by some authors. Instead of just focusing on the growth-inhibiting properties of the compounds, we aimed to assess whether they could inhibit antibiotic tolerance and thus improve the efficacy of rifampicin against biofilms.

In this study, NSAID-CAIs were assessed against attenuated H37Ra Mtb and its closely related species *Mycobacterium marinum* (Mmr). Mmr is a natural pathogen of zebrafish (*Danio rerio*), to which it causes a well-characterized TB-like infection [23,24]. Mmr has orthologs for the three Mtb β-CAs: MMAR_4135 (with 84.66% protein sequence identity) orthologous to β-CA1, MMAR_5088 (86.34%) for β-CA2, and MMAR_1266 (73.09%) for β-CA3.

2. Results

2.1. Design and synthesis of compounds

Compounds **1**–**5**, **7**–**10**, **12**–**16**, **18**–**23**, and **25**–**27** were synthesized in accordance with the experimental procedures previously reported by some of us (Fig. 1) [15].

The same approach was applied to the synthesis of (±)-fenoprofen derivatives **6, 11**, **17**, and **24**, which are reported here for the first time. We used the carboxylic acid moiety present in the clinically used and commercially available NSAID (±)-fenoprofen to efficiently install the primary sulfonamide and CA-directed warhead by means of an amide linkage (Fig. 2).

Like the derivatives previously reported [15], the connecting moieties in **6**, **11**, **17**, and **24** are thought to be cleaved when the compound is exposed to a granulomatous environment rich in hydrolytic enzymes [11]. All final compounds considered in this study were characterized by means of ^{1}H and ^{13}C NMR spectroscopy and HRMS and were ≥96% pure by elemental analysis (Supplementary Fig. S1).

2.2. In vitro carbonic anhydrase inhibition assay

Compounds **1**–**27** and the standard CAI acetazolamide (AAZ) were assessed for their ability to inhibit Mtb β-CAs 1-3 as well as hCA isoforms IX and XII via a stopped-flow CO_2 hydration assay [25]. The data are reported in Table 1 as K_I values. Supplementary Table ST1 reports the K_I data of **1**–**27** relative to the broadly expressed hCA isoforms I and II. Based on the kinetic data reported in Table 1, the following structure–activity relationships (SARs) for each enzymatic isoform can be drawn.

i) Mtb β-CA1: Among the sulfanilamide series (compounds **1**–**6**), (±)-naproxen **2** and diclofenac **5** derivatives were the most efficient inhibitors, with K_Is of 5.40 and 5.68 μM, followed by (±)-flurbiprofen **4** (K_I of 7.58 μM). CAIs bearing (±)-ketoprofen **3** and (±)-ibuprofen **1** tails showed similar inhibition potencies (K_Is of 17.5 and 21.4 μM, respectively). Finally, (±)-fenoprofen **6** was the least effective inhibitor of this isoform, with a K_I value of

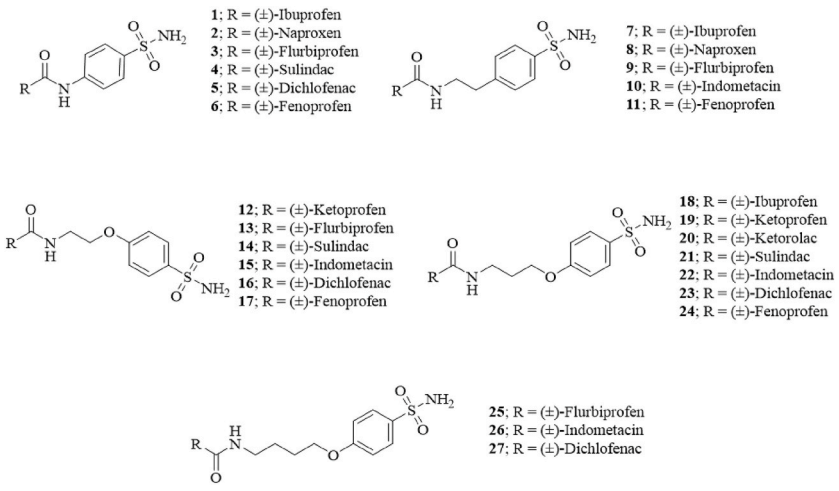

Fig. 1. Chemical structures of compounds 1-27 considered in this study [15].

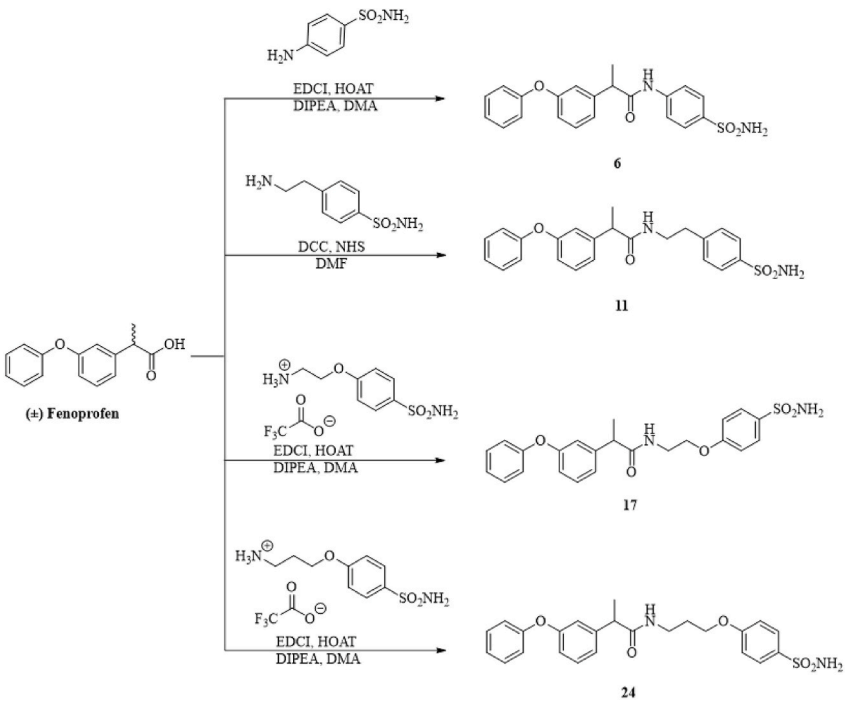

Fig. 2. Synthesis of (±)-fenoprofen derivatives 6, 11, 17 and 24.

Table 1
Inhibition data of NSAID-CAIs **1**–**27** on Mtb β-CAs 1-3 and hCAs IX and XII by the stopped-flow CO_2 hydrase assay [25].

K_I (μM)[a]					
Compound	**β-CA1**	**β-CA2**	**β-CA3**	**hCA IX**	**hCA XII**
1	21.4 (±0.02)	48.0 (±0.2)	2.18 (±0.05)	0.014 [15]	0.033 [15]
2	5.40 (±0.11)	0.083 (±0.03)	3.67 (±0.41)	0.019 [15]	0.029 [15]
3	17.5 (±0.32)	0.901 (±0.41)	0.972 (±0.03)	0.009 [15]	0.040 [15]
4	7.58 (±0.21)	4.6 (±0.34)	3.69 (±0.07)	0.061 [15]	0.027 [15]
5	5.68 (±0.42)	0.302 (±0.03)	0.95 (±0.02)	0.005 [15]	0.007 [15]
6	43.4 (±0.32)	3.4 (±0.02)	2.33 (±0.03)	0.024 (±0.06)	0.010 (±0.01)
7	62.9 (±0.09)	0.086 (±0.002)	5.43 (±0.04)	0.072 [15]	0.094 [15]
8	60.4 (±0.04)	0.083 (±0.01)	0.971 (±0.02)	0.005 [15]	0.003 [15]
9	9.24 (±0.03)	0.078 (±0.02)	8.25 (±0.01)	0.038 [15]	0.093 [15]
10	41.9 (±0.08)	0.343 (±0.02)	3.46 (±0.01)	0.063 [15]	0.093 [15]
11	50.6 (±0.04)	0.865 (±0.03)	4.19 (±0.12)	0.030 (±0.02)	0.007 (±0.03)
12	>100	0.162 (±0.02)	28.2 (±0.14)	0.077 [15]	0.009 [15]
13	>100	0.085 (±0.03)	59.2 (±0.12)	0.244 [15]	0.069 [15]
14	79.8 (±0.21)	0.094 (±0.01)	9.06 (±0.08)	0.103 [15]	0.065 [15]
15	89.2 (±0.07)	0.089 (±0.02)	28.2 (±0.09)	0.177 [15]	0.044 [15]
16	>100	0.081 (±0.02)	7.81 (±0.05)	0.144 [15]	0.058 [15]
17	>100	0.080 (±0.01)	6.73 (±0.11)	0.081 (±0.01)	0.052 (±0.03)
18	51.5 (±0.2)	0.270 (±0.03)	24.2 (±0.08)	0.010 [15]	0.007 [15]
19	>100	0.210 (±0.01)	7.34 (±0.03)	0.010 [15]	0.005 [15]
20	78.5 (±0.09)	0.094 (±0.02)	7.98 (±0.10)	0.018 [15]	0.007 [15]
21	>100	0.166 (±0.02)	55.0 (±0.07)	0.141 [15]	0.035 [15]
22	>100	0.085 (±0.03)	45.2 (±0.05)	0.202 [15]	0.084 [15]
23	>100	0.093 (±0.01)	40.5 (±0.08)	0.137 [15]	0.059 [15]
24	83.4 (±0.24)	0.170 (±0.06)	31.6 (±0.09)	0.018 (±0.01)	0.014 (±0.01)
25	>100	0.089 (±0.03)	8.09 (±0.01)	0.046 [15]	0.094 [15]
26	48.8 (±0.03)	0.091 (±0.01)	8.72 (±0.16)	0.008 [15]	0.064 [15]
27	>100	0.092 (±0.02)	7.55 (±0.18)	0.052 [15]	0.094 [15]
AAZ	0.480 (±0.02)	0.009 (±0.01)	0.104 (±0.02)	0.026 (±0.01)	0.006 (±0.01)

[a] Mean ± SD from 3 different assays, by a stopped flow technique.

43.4 μM. Elongation of the linear tether up to two carbon atoms, as for compounds **7**–**11**, increased all associated K_I values, except for the (±)-flurbiprofen derivative **9**, which was 1.9-fold more potent than its shorter progenitor compound **3.** Further elongation of the tether by the insertion of an oxygen atom, as in derivatives **12**–**17**, greatly spoiled the inhibition potencies. The sulindac **14** and indomethacin **15** derivatives were the only ones that maintained discriminate K_I values of 79.8 and 89.2 μM, respectively. A similar kinetic trend was observed for long derivatives **18**–**24.** Among this series, (±)-ibuprofen **18**, (±)-ketorolac **20**, and (±)-fenoprofen **24** showed inhibition values of 51.5, 78.5, and 83.4 μM, respectively, whereas all the other compounds were ineffective. Finally, among the longest

derivatives (**25**–**27**), indomethacin-CAI **26** was the only Mtb β-CA1 inhibitor (K_I of 48.8 μM).

ii) Overall, compounds **1**–**27** were more effective inhibitors of the Mtb β-CA2 isoform than the β-CA1 isoform mentioned above. (±)-Ibuprofen-sulfanilamide derivative **1** was the least effective among all the series considered, with a K_I value of 48.0 μM. Within the sulfanilamide series, compound **1** was followed by sulindac **4** and (±)-fenoprofen **6** derivatives (K_Is of 4.6 and 3.4 μM**,** respectively). (±)-Naproxen-sulfanilamide **2** was the most potent inhibitor among the sulfanilamide series (**1**–**6**), with a K_I of 0.083 μM. Substitution of the NSAID tail from (±)-flurbiprofen **3** to diclofenac **5** resulted in a 3.0-fold increase in the inhibition potency (K_Is of 0.901 and 0.302 μM**,** respectively). The introduction of an ethyl linker decreased the K_I values for the (±)-ibuprofen **7**, (±)-flurbiprofen **9**, and (±)-fenoprofen **11** derivatives compared with their shorter analogs **1**, **3**, and **6** (K_Is of 0.086, 0.078, and 0.865 μM for **7**, **9**, and **11,** respectively). Interestingly, elongation of the tether did not affect the inhibitory potency of the (±)-naproxen NSAID for Mtb β-CA2 (K_Is of 0.083 μM for **2** and **8**). Indomethacin-CAI **10** was a submicromolar inhibitor with a K_I of 0.343 μM. Among the phenoxy series **12**–**17**, (±)-ketoprofen derivative **12** was the least effective inhibitor of Mtb β-CA2, with a K_I value of 0.162 μM. All the other compounds (**13**–**17)** were effective by up to 2.3-fold compared with **12**, with K_I values quite close to each other and ranging between 0.080 and 0.094 μM. Among the elongated derivatives **18**–**24**, (±)-ibuprofen **18** had the highest K_I value within the series (K_I of 0.270 μM), followed by (±)-ketoprofen **19**, which was 1.3-fold less potent (K_I of 0.210 μM). Sulindac **21** and (±)-fenoprofen **24** were almost equally potent inhibitors of the Mtb β-CA2 isoform (K_Is of 0.166 and 0.170 μM**,** respectively). A similar trend was observed for the (±)-ketorolac **20** and diclofenac **23** derivatives, as they presented K_Is of 0.094 and 0.093 μM, respectively. Indomethacin **22** was the most effective inhibitor among this series, as it had a K_I value of 0.085 μM. The longest derivatives **25**–**27** were submicromolar inhibitors with K_I values ranging between 0.089 and 0.092 μM; thus, no appreciable differences were observed in the extraction of proper SARs.

iii) The NSAID-CAI derivatives **1**–**27** showed marked differences when profiled on Mtb β-CA3. Compounds in the sulfanilamide series (**1**–**6**) exhibit superimposable K_Is as pairs. For example, the (±)-naproxen **2** and sulindac **4** derivatives were equipotent inhibitors (K_Is of 3.67 and 3.69 μM**,** respectively), followed by (±)-ibuprofen **1** and (±)-fenoprofen **6** (K_Is of 2.18 and 2.33 μM**,** respectively), and then (±)-flurbiprofen **3** and diclofenac **5** (K_Is of 0.972 and 0.950 μM**,** respectively), which were the most effective pairs. Elongation of the sulfanilamide-containing series to afford derivatives **7**–**11** strongly affected the kinetic trend. The compounds (±)-ibuprofen **7**, (±)-flurbiprofen **9** and (±)-fenoprofen **11** were 2.5-, 2.2-, and 1.8-fold less effective than their shorter counterparts **1**, **3**, and **6** (K_Is of 5.43, 8.25, and 4.19 μM for **7**, **9**, and **11,** respectively). Interestingly, elongation of the tether was beneficial only for the (±)-naproxen-containing compounds, as **8** was 3.8-fold more potent than **2** (K_Is of 3.67 and 0.971 μM for **2** and **8,** respectively). Finally, indomethacin **10** was a low micromolar inhibitor of Mtb β-CA3 with a K_I of 3.46 μM. Wider distributions of the K_I values were obtained for phenoxy series **12**–**17** and **18**–**24**, thus allowing us to decipher appropriate SARs. Within the first series, diclofenac **16** and (±)-fenoprofen **17** were the most effective inhibitors, with K_I values of 7.81 and 6.73 μM, respectively, followed by sulindac **14**, with a K_I of 9.06 μM. Interestingly, the increase in potency between pairs **16**/**17** and **14**/**17** were the same (1.16-fold). Both (±)-ibuprofen **12** and indomethacin **15** derivatives were equipotent inhibitors (K_Is of 28.2 μM), whereas (±)-flurbiprofen **13** was effective only at medium micromolar concentrations (K_I of 59.2 μM). Further elongation of the alkyl tether, as in the compound series **18**–**24**, led to evident changes in the kinetic values. For example, (±)-ketoprofen derivative **19** was 3.8-fold more effective in inhibiting Mtb β-CA3 than its shorter analog **12** (K_Is of 28.2 and 7.34 μM for **12** and **19,** respectively). The other compounds, **21**–**24**, presented markedly lower potencies than their shorter analogs, **14**–**17.** Specifically, sulindac **21** was 6.1-, indomethacin **22** 1.6-, diclofenac **23** 5.2-, and (±)-fenoprofen **24** 4.7-fold less effective than each shorter counterpart. (±)-Ibuprofen **18** and ketorolac **20** had K_I inhibition values of 24.2 and 7.98 μM, respectively. Interestingly, the longest compounds considered in this study (**25**–**27**) were low micromolar inhibitors of Mtb β-CA3, and the K_I values were very close to each other (7.55-8.72 μM); thus, any consideration of the SAR was not feasible.

iv) The (±)-fenoprofen derivatives **6**, **11**, **17**, and **24** were profiled *in vitro* on hCAs I, II, IX, and XII, and the associated K_I values agreed with previously reported NSAID-CAIs [15]. The kinetic data associated with hCAs I and II are reported in Supplementary Table S1. The hCA isoforms IX and XII, which are implicated in inflammation events, were effectively inhibited at low micromolar concentrations, with small differences among the compounds. For example, hCA IX had K_I values of 0.018-0.030 μM for **6**, **11**, and **24**, whereas derivative **17** was a 0.081 μM inhibitor. A similar kinetic trend, although with lower K_Is, was reported for the hCA XII isoform. In this case, compounds **6**, **11**, and **24** presented K_I values between 0.007 and 0.014 μM, and derivative **17** was effective at 0.052 μM. For the hCA I isoform, the K_I values ranged between 0.47 and 0.889 μM, except for **24,** for which the inhibition efficacy was 3.28 μM. Similarly, hCA II included compounds **6**, **11**, and **17** as inhibitors in the low nanomolar concentration range (K_Is between 2.0 and 8.0 nM), except for **24,** which was effective at high nanomolar concentrations (K_I of 332.0 nM).

During the writing of the manuscript, the authors predicted the expression of an Mtb γ-CA isoform via bioinformatic approaches [26]. Experimental evidence of such an isoform has yet to be reported, including determination of its role in bacterial survival and infection processes; thus, it is not included in this investigation.

2.3. NSAID-CAIs have antimycobacterial activity

The antimycobacterial assessment of NSAID-CAIs was conducted on H37Ra Mtb along with Mmr, an ideal and reliable model organism for conducting *in vitro* mycobacterial screenings, as Mmr grows faster than does Mtb and is easier to handle in BSL2 laboratories. To assess whether NSAID-CAIs and their constitutive single entities, NSAIDs and CAIs (i.e., (±)-ibuprofen, (±)-ketoprofen, (±)-flurbiprofen, (±)-fenoprofen, 4-(2-aminoethyl)benzenesulfonamide, 4-(3-aminopropoxy)benzenesulfonamide, 4-(2-aminoethoxy)benzenesulfonamide, and 4-(4-aminobutoxy) benzenesulfonamide), inhibit mycobacterial growth, we conducted traditional MIC testing in both planktonic and biofilm culture environments [27,28]. To study the bacteriostatic properties, we treated cultures before the start of the exponential growth phase. Mycobacterial burdens were quantified before starting treatment and were $3.26 \pm 1.54 \times 10^5$ CFU/ml for Mmr and $2.17 \pm 0.49 \times 10^5$ CFU/ml for H37Ra Mtb. NSAID-CAIs **7**, **9**, **11**, **12**, **13**, **17**, **18**, **19**, **24**, and **25** and their single fragments were used at concentrations ranging between 12.5 and 200 μM for the former and up to 400 μM for the latter.

The obtained data are shown in Supplementary Fig. S2**,** with the MIC_{50} values for each NSAID-CAI shown in separate graphs. All ten NSAID-CAIs had noticeable inhibitory efficacy. Among the three experimental conditions, the best inhibition was achieved with H37Ra Mtb biofilm medium, followed by Mmr biofilm medium and, finally, planktonic Mmr cultures. In H37Ra Mtb biofilms, the top two compounds with the lowest MIC_{50} values were **25** (11.26 μM) and **24**

(11.55 μM). MIC_{50} values below 100 μM were achieved with most NSAID-CAIs (**25**, **24**, **13**, **11**, **19**, **17**, and **18**). Testing was performed for NSAID and CAI fragments accordingly, with MIC_{50} values against Mmr in biofilm medium shown in Supplementary Fig. S2. These fragments performed poorly in comparison to hybrid compounds, with at least doubled MIC_{50}s (excluding (±)-fenoprofen, with an MIC_{50} of 151.5 μM).

Next, we screened the entire compound panel through an MDK assay, which allows the survival of tolerant bacterial subpopulations to be measured. The assay is based on ATP-coupled bioluminescence reporters, which enable high-throughput, noninvasive detection of live mycobacteria expressing *luciferase* genes [2]. Unlike the MIC assay, the starting point for the measurement is mycobacteria in the saturated stationary growth phase. The MDK assay was performed at a fixed concentration of bioluminescent Mmr and H37Ra Mtb. The AUCs of the time–kill curves were compared to those of the untreated control and are displayed as relative values on a logarithmic scale, as plotted in Fig. 3. Ten compounds (**7**, **9**, **11**, **12**, **13**, **17**, **18**, **19**, **24**, and **25**) significantly reduced the Mmr biofilm AUC ($p < 0.001$) to less than one-tenth of the AUC observed in untreated culture (Fig. 3 A). Furthermore, derivatives **13** ($p = 0.039$), **18** ($p = 0.011$), **19** ($p = 0.031$) and **24** ($p = 0.015$) had AUCs that were significantly smaller than those of the rifampicin-treated (487 μM) control culture.

Luminescence reduction induced by the ten NSAID-CAIs evolved in a dose-dependent manner in Mmr biofilms. The dose–dependent MDK time–kill curves are shown in Supplementary Fig. S3. Four compounds were able to surpass the MDK_{99} threshold (2-log_{10}-fold reduction), at which less than 1% of the luminescence remained within the 7-day follow-up period. At the highest concentration (200 μM), MDK_{99} was reached at 24 h by compound **24**, at 72 h by compound **13**, at 96 h by compound **19,** and at 144 h by compound **17**. Notably, the reduction in luminescence induced by compound **24** reached the $MDK_{99.9}$ threshold (3-log_{10}-fold reduction) at 120 h. At 100 μM, MDK_{99} was reached at 72 h by compound **24**, at 120 h by compound **19** and at 168 h by compound **17**. Finally, treatment with either compound **19** or **24** at 50 μM surpassed the MDK_{99} threshold at 144 h.

The efficacy of these ten compounds against biofilm cultures was greater than that against planktonic cultures (Fig. 3 A). Planktonic Mmr cultures treated with equal doses of NSAID-CAIs retained more bioluminescence, as only compounds **12**, **19**, and **24** reduced the AUC to less than one-tenth of the untreated control AUC ($p < 0.001$). Significance

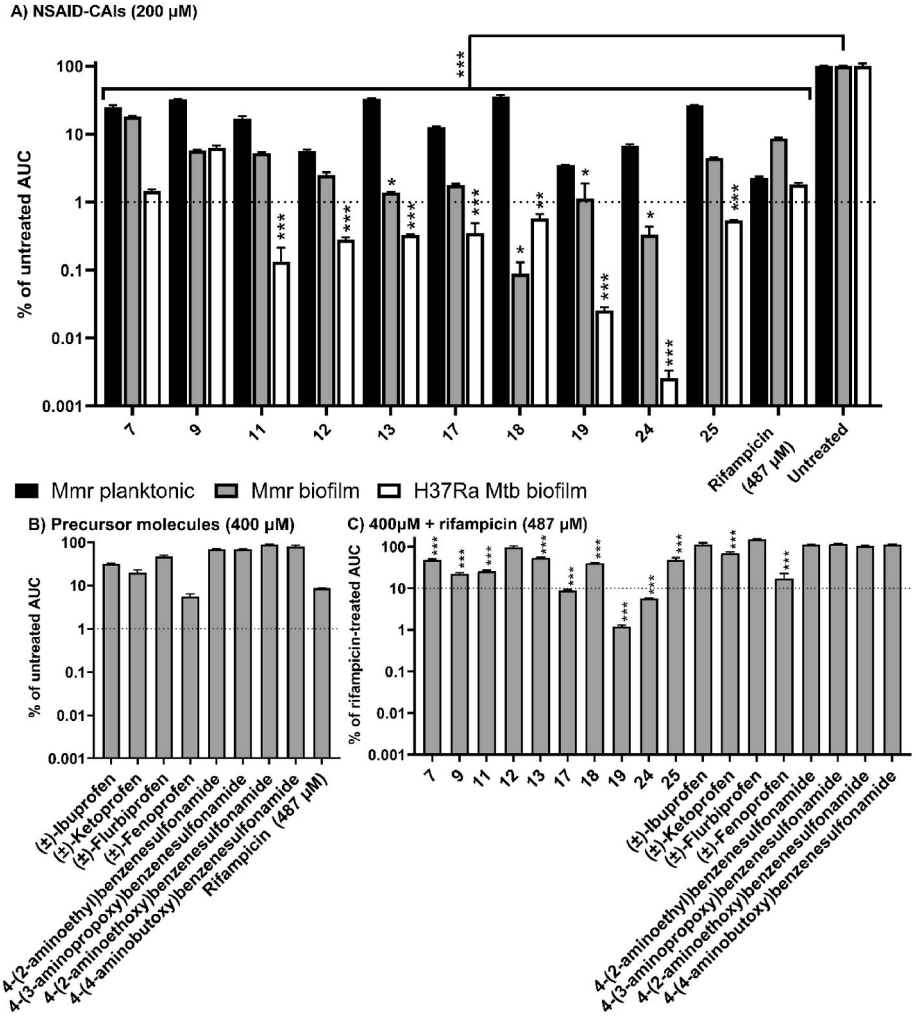

Fig. 3. NSAID–CAI hybrid molecules efficiently reduce mycobacterial bioluminescence, but the same does not translate into precursor molecules. A) NSAID-CAIs (200 μM) decrease mycobacterial metabolically coupled bioluminescence in all three test environments. B) NSAID or CAI fragments (400 μM) do not reach similar levels of reduction in Mmr biofilms. C) Several hybrids potentiate the effects of rifampicin. Bar graphs represent the time–kill curve (24-96 h post-treatment) AUCs (mean ± SD) on a log_{10} scale, normalized against the untreated mycobacterial AUC in A) and the B) or rifampicin (487 μM)-treated AUC in C). The dotted line indicates a 99% reduction in A) and B) and a 90% reduction in C). Column color indicates the mycobacterial culture; the black bars indicate planktonic Mmr, the gray Mmr biofilms and the white H37Ra Mtb biofilms. Each treatment was measured in biological triplicates. Significance was determined by comparing samples to the rifampicin (487 μM) control via one-way ANOVA and Dunnett's post hoc tests. * Indicates $p < 0.05$, ** indicates $p < 0.01$ and *** indicates $p < 0.001$.

against the rifampicin (487 μM) control was not observed, as the AUCs remained larger than those of rifampicin. Importantly, the NSAID-CAIs showed the greatest efficacy against H37Ra Mtb biofilms, as all ten compounds had significantly ($p < 0.001$) reduced AUCs in comparison with those of the untreated control (Fig. 3 A). All ten compounds had AUCs less than one-tenth of the untreated AUC, and compounds **11**, **12**, **17**, **18** and **25** had AUCs less than one percent. Furthermore, the most effective derivatives, **19** and **24**, had AUCs less than 0.1% of the control AUC. Compared with the rifampicin-treated (487 μM) H37Ra Mtb biofilm, derivatives **11**, **12**, **13**, **17**, **18**, **19**, **24**, and **25** had significantly lower AUCs ($p < 0.001$).

Like Mmr, NSAID-CAI activity in H37Ra Mtb evolved in a dose-dependent manner, as shown by the MDK time–kill curves displayed in Supplementary Fig. S4. Nine out of the ten NSAID-CAIs surpassed the MDK_{99} threshold during the measurement period. At 200 μM, MDK_{99} was 24 h for compounds **11**, **12**, **13**, **17**, **18**, **19**, **24**, and **25**, in addition to 144 h for compound **7**. At 100 μM, MDK_{99} was 24 h for compounds **17**, **19**, and **24**; 48 h for compound **11**; 72 h for compounds **12** and **25**; and 144 h for compound **13**. Even more, compound **19** (50 μM) surpassed the MDK_{99} threshold at 144 h. Comparably to Mmr biofilms, compound **24** at 200 μM reached the $MDK_{99.9}$ threshold by 168 h, making this NSAID-CAI the most potent compound according to the bioluminescence assessment. Overall, the MDK data revealed that compounds **7**, **9**, **11**, **12**, **13**, **17**, **18**, **19**, **24**, and **25** were far more effective at decreasing the luminescence of the Mmr and H37Ra Mtb biofilm cultures than the planktonic Mmr cultures. Notably, preferential activity against H37Ra Mtb over Mmr was observed, with derivatives **11**, **19**, and **24** showing the highest efficacy among all the tested compounds (Fig. 3 A).

The MDK screening of the NSAID and CAI fragments at 400 μM revealed (±)-fenoprofen as the sole molecule to reduce the time–kill curve AUC below one-tenth of the untreated control AUC (Fig. 3 B) ($p < 0.001$). Compared with rifampicin treatment (487 μM), none of the fragments had a significantly reduced AUC, nor did they reach the MDK_{99} threshold during the seven-day measurement (Supplementary Fig. S5). Individual fragments induce far less reduction in Mmr bioluminescence, indicating that the efficacy is derived from either the synergy or hybridization of these fragments.

Next, the Mmr biofilm MDK assay was carried out by combining each of the ten NSAID-CAIs (400 μM) with rifampicin (487 μM). Compounds **17**, **19**, and **24** were able to reduce the AUCs to less than one-tenth of the rifampicin-treated AUCs ($p < 0.001$), thus potentiating its activity (Fig. 3C). Significantly reduced AUCs were also found with rifampicin combined with compounds **7**, **9**, **11**, **13**, **18**, and **25** ($p < 0.001$). Interestingly, two of the NSAID fragments, (±)-ketoprofen and (±)-fenoprofen, significantly reduced the AUC ($p < 0.001$). The time–kill curves revealed that rifampicin treatment (487 μM) reached the MDK_{99} threshold at 96 h. NSAID-CAIs that reduced the time needed to surpass this threshold were **9**, **17**, **19**, and **24** (MDK_{99} at 24 h); **11** (at 48 h); and **13**, **18**, and **25** (at 72 h) (Supplementary Fig. S6). The NSAID (±)-fenoprofen reduced the time needed to reach MDK_{99} to 24 h.

To further evaluate whether the efficacy comes from fragment hybridization, we coadministered MDK-assayed NSAIDs and CAIs at a 1/1 ratio at a final concentration of 100 μM (Fig. 4). Compared with their constitutive fragments individually or in combination, compounds **11**, **19**, and **24** had a significantly greater ability to reduce the bioluminescence in both the Mmr (Fig. 4 A) and H37Ra Mtb (Fig. 4 B) biofilms ($p < 0.001$). These experiments provide the first scientific evidence that moderate dosages of dual-acting NSAID-CAIs are far more effective at inhibiting mycobacterial metabolism and thus inducing cellular death than combinations of their individual chemical components. Particularly relevant for this study is the preferential activity of such compounds for H37Ra Mtb over the Mmr biofilm, thus providing value for their potential therapeutic application.

2.4. Toxicity assessment of NSAID-CAIs

The toxicity profiles of compounds **7**, **9**, **11**, **12**, **13**, **17**, **18**, **19**, **24**, and **25** were assessed by immersing 1 dpf zebrafish embryos in increasing concentrations of each compound ($n = 20$ embryos per group). The corresponding LC_{50}s and mortality percentages were calculated after four days of exposure and are reported in Supplementary Table ST2. Overall, NSAID-CAI concentrations ≥400 μM were associated with high mortality. Hybrids containing (±)-fenoprofen (**11**, **17**, and **24**) induced mortality at concentrations ≥100 μM. These data, combined with the identification and characterization of any observable developmental defects in the larvae, allowed us to determine safely administrable dosages of NSAID-CAIs for further *in vivo* investigations. Fig. 5A–J shows representative phenotypic images of 5 dpf larvae after exposure to NSAID-CAIs at sublethal concentrations, and

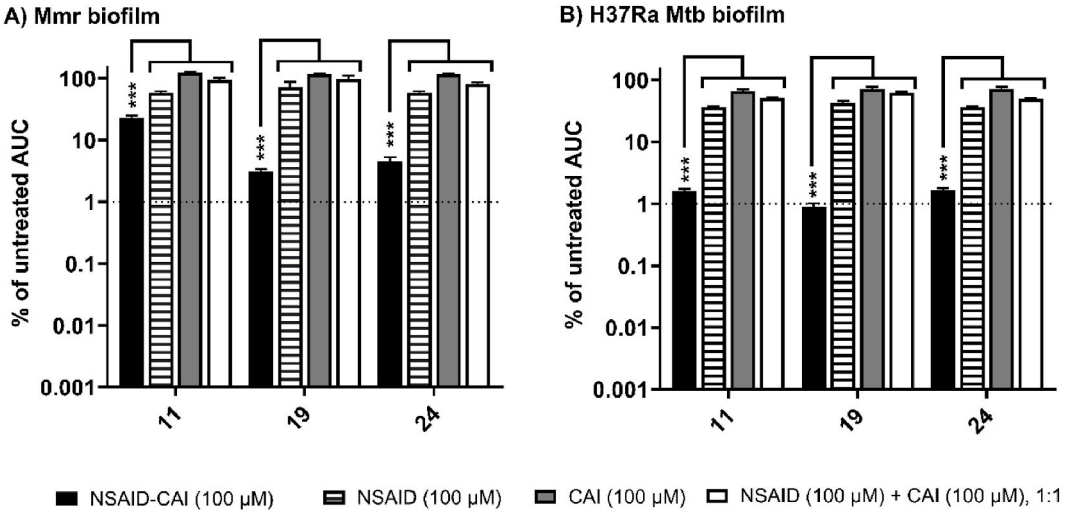

Fig. 4. The combination of NSAIDs and CAIs decreases luminescence less than NSAID-CAI hybrids do in both A) Mmr and B) H37Ra Mtb biofilms. Time–kill curve analysis was performed for derivatives **11**, **19**, and **24** and their chemical components. For the analysis, a concentration of 100 μM was used. Bar graphs represent the time–kill curve (24–96 h post-treatment) AUCs (mean ± SD) on a $\log_{10}$ scale, normalized against untreated biofilm culture AUCs. The dotted line indicates a 99% reduction in bioluminescence. The color of the columns indicates the treatment type; the black bars indicate hybrid molecules, the white with horizontal lines NSAID precursors, the gray CAI precursors and the white NSAID and CAI precursors in combination treatment. Each treatment was measured in biological triplicates. Significance was determined via two-way ANOVA and Tukey's post hoc test. *** Indicates $p < 0.001$.

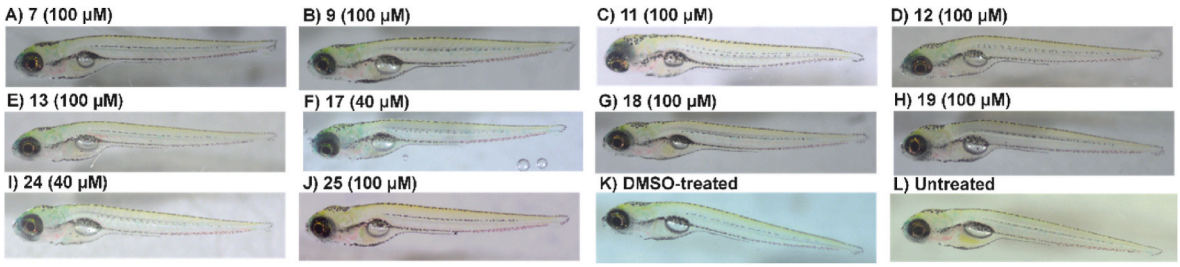

Fig. 5. Representative images of the phenotypes of 5 dpf zebrafish larvae after NSAID-CAI exposure. The images were taken at the highest concentration that does not cause mortality and results in seemingly normal development.

Figure K and L show phenotypes for negative controls. Visual inspection clearly revealed normal larval development with no visible defects, thus suggesting that NSAID-CAIs are highly tolerable *in vivo* and have high safety margins.

A similar toxicity assessment was subsequently performed for the NSAID and CAI fragments. NSAIDs cause substantial toxicity, with (±)-ibuprofen, (±)-ketoprofen, and (±)-flurbiprofen having LC_{50} values < 100 μM. (±)-Fenoprofen was the least toxic NSAID, with an LC_{50} of 141.6 μM. CAIs were better tolerated, with LC_{50} values ranging between 153.5 and 292 μM. The corresponding LC_{50}s and mortality percentages of the constitutive fragments are reported in Supplementary Table ST3.

2.5. Assessment of bactericidal antimycobacterial activity

The bactericidal activities of NSAID-CAIs **7**, **9**, **11**, **12**, **13**, **17**, **18**, **19**, **24**, and **25** were evaluated by daily quantification of changes in the number of colony-forming units (CFUs) on the Mmr biofilm. We plotted time–kill curves of treated Mmr biofilm samples and compared the AUCs as previously described in section 3.3, which were only based on the bacterial load rather than the RLU. Each NSAID-CAI was tested at a single dose of 100 μM (Fig. 6 A) in combination with 487 μM rifampicin (Fig. 6 B), as this concentration was well tolerated in the toxicity assessment (3.4.). Three compounds, **11** ($p = 0.0044$), **19** ($p < 0.001$), and **24** ($p < 0.001$), were significantly bactericidal on their own. Similar trends were observed for compounds **7**, **9**, **17**, and **18**, which had reduced AUCs, although the differences were not statistically significant. Compound **12** ($p = 0.0163$) was the only compound that significantly potentiated the effects of rifampicin. Additionally, compounds **9**, **11**, **12**, **18**, and **19** in combination with rifampicin had lower AUCs than rifampicin alone.

2.6. Antibacterial assessment of NSAID-CAIs in an adult zebrafish TB model

Finally, we aimed to study the antibacterial efficacy of NSAID-CAIs in an *in vivo* adult zebrafish model. Among the ten selected NSAID-CAIs, derivatives **12** and **19** had great inhibitory effects in MDK assays, were safe for use with zebrafish larvae, and exhibited promising bactericidal potential alone or when combined with rifampicin; thus, these derivatives were selected as *proof-of-concept* candidates to assess any *in vivo* antibacterial effects on an adult zebrafish infection model. A total of 239 adult AB zebrafish aged 5–13 months were infected (*i.p.*) with 56 ± 12 CFUs of Mmr, and among them, 4 individuals were euthanized at the humane endpoint prior to the daily oral administration of compound **12** (68 mg/kg) and rifampicin (32 mg/kg) or compound **19** (70 mg/kg) and rifampicin (32 mg/kg). During the experiment, 5 individuals from the rifampicin-treated group, 10 individuals from the compound **12** and rifampicin-treated groups and 7 individuals from the compound **19** and rifampicin-treated groups were euthanized for infection symptoms. All zebrafish were assumed to be male. During organ collection, 5 individuals across the groups were found to be female. The difference between female and male zebrafish bacterial burdens was assumed to be insignificant; thus, the results were analyzed as one dataset. The median bacterial burden at 4 wpi, just before starting treatment, was 389,167 (IQR 193,944-978,333) CFU/fish ($n = 20$). During plating, all samples treated with compound **19** and rifampicin at 6 wpi were incorrectly processed, and the results were thus excluded from the study. The analysis of samples exposed to the combination of compound **12** and rifampicin revealed a greater median number of CFUs ($p = 0.73$) than samples treated only with rifampicin at 6 wpi, indicating that compound **12** does not add efficacy within the first

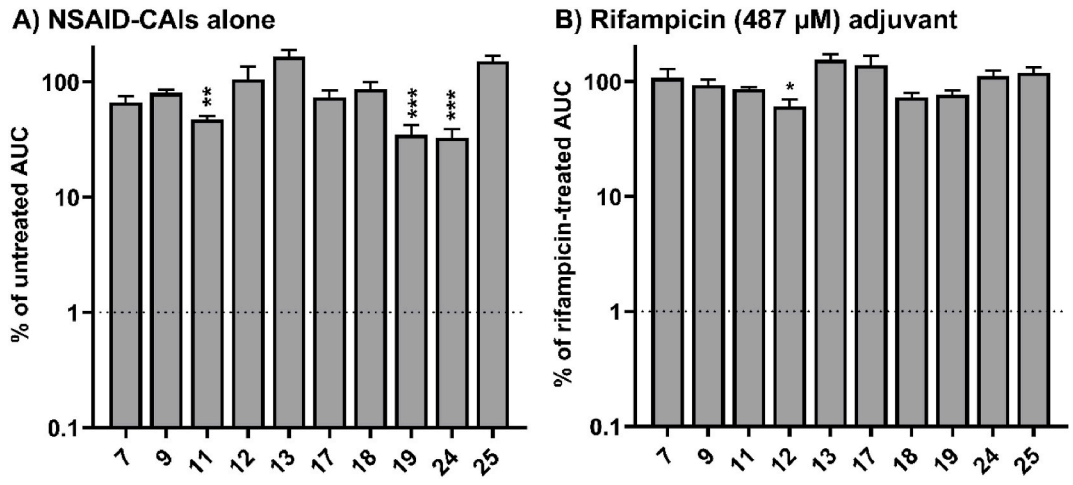

Fig. 6. Some NSAID-CAIs have bactericidal effects on Mmr biofilm cultures. For the analysis, 100 μM NSAID-CAIs were used. Bar graphs represent the time–kill curve (24 to 96 h post-treatment) AUCs (mean ± SD) on a $\log_{10}$ scale, normalized against untreated Mmr biofilms in A) or rifampicin (487 μM)-treated biofilms in B). Each treatment was measured in biological triplicates, and the dotted line indicates a 99% reduction in CFUs. Significance was determined with one-way ANOVA and Dunnett's post hoc test; * indicates $p < 0.05$, ** indicates $p < 0.01$ and *** indicates $p < 0.001$.

two weeks of treatment. After four weeks of treatment at 8 wpi, the bacterial burden in the rifampicin-treated group was 578,333 (IQR 108,083-1,479,167) CFU/fish (Fig. 7) (n = 20). The median (IQR) bacterial burden in the fish treated with compound **19** and rifampicin was 916,667 (265,417–1,866,667) CFU/fish (p = 0.34, n = 20). Similarly, the median bacterial burden in the fish treated with compound **12** and rifampicin was 570,833 (IQR 241,250-2,318,750) CFU/fish (p = 0.70, n = 20). Two weeks later, at the experimental endpoint (10 wpi), the median bacterial burden in the rifampicin-treated group was 900,833 (IQR 563,333-4,708,333) CFU/fish (n = 24). The median bacterial burden was 866,667 (IQR 368,750-2,641,667) CFU/fish (p = 0.47) in fish treated with compound **19** and rifampicin (n = 24) and 852,917 (IQR 389,583-2,795,833) CFU/fish (p = 0.58) in fish treated with compound **12** and rifampicin (n = 20).

Fig. 7 shows the distribution of individual bacterial burdens. Statistical significance was assessed via Mann–Whitney tests; however, significance was not achieved, as the results were largely skewed by high variation between individuals. This heterogeneity is reasonably attributed to the lengthy experiments, which amplify the intrinsic variability in infection progression among individuals, especially when animals of different age are included. Additionally, as NSAID-CAIs and rifampicin are mixed with fish food, a source of variation may arise from the uneven distribution of compounds within the food particles and uneven consumption of the food. The level of absorption from the fish gut remains unknown and is likely relatively low. As statistical significance was not reached, no conclusions regarding a reduction in bacterial burden can be drawn.

3. Discussion

TB remains a health threat to millions each year. Moreover, drug resistance is a problem for infection control, creating a demand for treatment alternatives in addition to traditional drugs. Here, we assessed the antimycobacterial activity of NSAID-CAI types **1**–**27** both *in vitro* and *in vivo* in an adult zebrafish infection model, with the aim of providing experimental evidence to validate the druggability of Mtb β-CAs 1-3, which was further supported by applying principles of the HDT approach. Compared with their single constitutive fragments, compounds **1**–**27**, which are endowed with enhanced host immune activity [15], efficiently inhibited the target Mtb β-CAs 1-3 *in vitro*, with associated K_I values in the low micromolar range. Overall, the best *in vitro* inhibition occurred against Mtb β-CA2, which has been predicted to be essential for Mtb survival [29]. Additionally, recent knockdown studies confirmed that β-CA2 has substantial effects on the growth and virulence of Mtb [30,31].

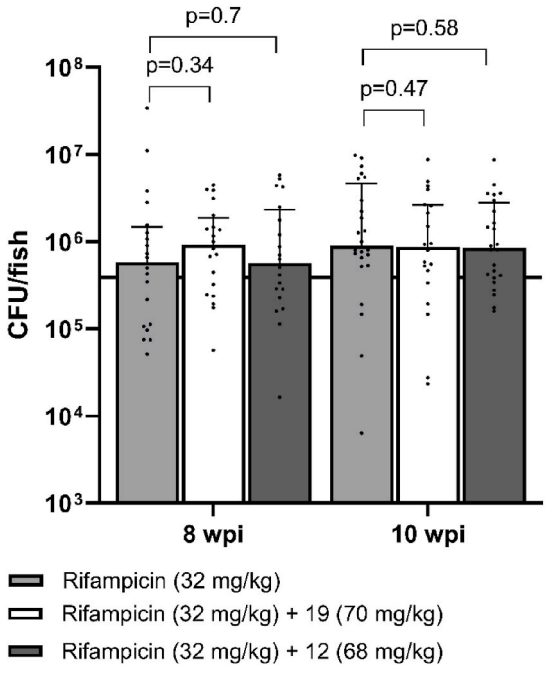

Fig. 7. Compared with rifampicin-treated zebrafish, combination therapy with rifampicin and NSAID-CAIs does not result in reduced bacterial burden. The infection was followed for 10 weeks, and the bacterial burden was quantified at 4, 8 and 10 wpi. The horizontal line indicates the median bacterial burden in untreated zebrafish at 4 wpi. Bar graphs represent the bacterial burden (median ± IQR) on a $\log_{10}$ scale. Each black dot represents the absolute Mmr-bacterial burden per individual fish. Statistical significance was determined with Mann–Whitney tests, p > 0.05 = not significant.

The antimycobacterial activities of compounds **1**–**27** were assessed via MDK time–kill curves since the measured ATP-mediated bioluminescence is a marker of cellular viability and correlates with CFU values [32,33]; thus, this method provides effective readouts of the activity of the compounds against tolerant bacteria. Importantly, preclinical TB research currently lacks studies targeting tolerant subpopulations. The results revealed that compounds **7**, **9**, **11**, **12**, **13**, **17**, **18**, **19**, **24**, and **25** reached the MDK_{99} threshold as early as the first day of treatment in both the Mmr and H37Ra Mtb biofilms in a dose-dependent manner. As a key finding, the efficacy in biofilms outperforms the moderate effects such compounds had in Mmr planktonic cultures. Previous studies have shown the presence and upregulation of β-CA2 in biofilm-forming conditions [2,6,22]. Thus, the inhibitory effect of NSAID-CAIs against β-CA2 could translate to interference in biofilm homeostasis.

In all cases, the *in vitro* antibacterial effect of each NSAID-CAI was far superior to that of the single constitutive fragments coadministered at the same concentration. We report, as another key finding, that the dual-acting NSAID-CAIs, synthesized via molecular linking, have enhanced inhibitory properties and safety profiles in comparison to their constitutive fragments. Compounds **11**, **19**, and **24** exhibited significant bactericidal properties, whereas compound **12** appeared to potentiate the bactericidal effect of rifampicin. Compounds **12** and **19** showed the best performance in terms of antimycobacterial efficacy and safety profiles and were tested in Mmr-infected zebrafish coadministered rifampicin orally, failing to reach statistically significant results. This is likely due to the large variation between individual samples that can arise from a variety of reasons, most probably being the difference between the infection progress of individuals of different ages. All in all, we are confident that the present experimental data provides solid evidence for the *in vitro* efficacy of NSAID-CAIs. This effect can be attributed to the inhibition of bacterial β-CAs, particularly the β-CA2 isoform, along with the possible suppression of the host immune response through induction of the HDT effect.

4. Methods

4.1. Chemistry

All anhydrous solvents and reagents used in this study were purchased from Alfa Aesar (MA, USA), TCI (Japan) and Sigma–Aldrich (MO, USA). The synthetic reactions involving air- or moisture-sensitive chemicals were carried out under a nitrogen atmosphere using dried glassware and syringes to transfer the solutions. Nuclear magnetic resonance (^{1}H NMR, ^{13}C NMR and ^{19}F NMR) spectra were recorded using an Avance III 400 MHz spectrometer (Bruker, MA, USA) with dimethyl sulfoxide (DMSO)-d_6 as the solvent. The chemical shifts are reported in parts per million (ppm), and the coupling constants (J) are expressed in Hertz (Hz). The splitting patterns are designated s, singlet; d, doublet; t, triplet; q, quartet; m, multiplet; brs, broad singlet; dd, doublet of doublets; and ddd, doublet of doublets of doublets. The correct assignment of exchangeable protons (i.e., OH and NH) was carried out by means of D_2O addition. Analytical thin-layer chromatography (TLC) was performed on silica gel F-254 plates (Merck KGaA, Germany).

Flash chromatography was performed on Merck silica gel 60 (230-400 mesh ASTM) as the stationary phase, and appropriate mixtures of ethyl acetate/n-hexane were used as the eluents. Melting points (m.p.) were measured in open capillary tubes with an MPD350.BM3.5 apparatus (Gallenkamp Labs, UK) and are uncorrected. The solvents used in the MS analyses were acetone, acetonitrile (Chromasolv grade), and mQ water (18 MΩ cm). High-resolution mass spectrometry (HRMS) analysis was performed with a Finnigan LTQ Orbitrap mass spectrometer (Thermo Fisher Scientific, MA, USA) coupled with an electrospray ionization source (ESI). Analysis was carried out in positive ion mode $[M + H]^+$, and proper dwell time acquisition was used to achieve 60,000 units of resolution at full width at half maximum. The elemental compositions of the compounds were calculated based on their measured accurate masses and only results with an attribution error of less than 2 ppm and a not integer RDB (double bond/ring equivalents) value were obtained. Stock solutions of analytes were prepared using acetone (1.0 mg mL^{-1}) and stored at 4 °C. The working solutions were diluted to mQ water/acetonitrile 1/1 (v/v) up to a concentration of 1.0 μg mL^{-1}. HRMS analysis was performed by introducing the analyte via a syringe pump at 10 μL min^{-1}. Sulfanilamide and 4-(2-aminoethyl)benzenesulfonamide are commercially available from Sigma–Aldrich. The 3-(4-sulfamoyl-phenoxy)-propyl-ammonium trifluoroacetic acid salt and 2-(4-sulfamoyl-phenoxy)-ethyl-ammonium trifluoroacetic acid salt were prepared as previously described [15].

4.2. General procedure for the synthesis of 6, 11, 17 and 24

(±)-Fenoprofen (1.0 eq.), 1-ethyl-3-(3-dimethylaminopropyl)carbodiimide hydrochloride salt (EDCI.HCl, 2.0 eq.) and 1-hydroxy-7-azabenzotriazole (HOAT, 2.0 eq.) were dissolved in dry dimethylformamide (DMF) or dimethylacetamide (DMA) (3.0 ml) and stirred for 10 min at room temperature, followed by the addition of corresponding amines [4-(2-aminoethyl)benzenesulfonamide, sulfanilamide, 3-(4-sulfamoyl-phenoxy)-propyl-ammonium trifluoroacetic acid salt or 2-(4-sulfamoyl-phenoxy)-ethyl-ammonium trifluoroacetic acid salt (2.0 eq.)] and *N,N*-diisopropylethylamine (DIPEA, 4.0 eq.) in the same solvent (1.5 ml). The mixture was stirred until consumption of the starting materials (TLC monitoring), quenched with an aqueous HCl solution (3.0 M) at 0–5 °C and extracted with ethyl acetate (3 × 15 ml). The combined organic layers were washed with an aqueous HCl solution (3.0 M), H_2O (3 × 20 ml), sat. aqueous $NaHCO_3$ (3 × 20 ml), dried over Na_2SO_4 and evaporated under vacuum to yield a residue that was purified by silica gel column chromatography, eluted with ethyl acetate/*n*-hexane, crystallized from ethyl acetate/petroleum ether or triturated from dichloromethane/petroleum ether to afford the title compounds.

4.3. 2-(±)-(3-Phenoxyphenyl)-N-(4-sulfamoylphenyl)propanamide 6

(±)-Fenoprofen (1.0 eq.), 1-ethyl-3-(3-dimethylaminopropyl)carbodiimide hydrochloride salt (EDCI. HCl, 2.0 eq.) and 1-hydroxy-7-azabenzotriazole (HOAT, 2.0 eq.), sulfanilamide (2.0 eq.) and *N,N*-diisopropylethylamine (DIPEA, 4.0 eq.) in dry DMF (4.5 ml) were treated according to the general procedure previously reported in section 2.1.1. The crude product was purified via silica gel column chromatography by elution with ethyl acetate/*n*-hexane 50% *v/v* and crystallized from ethyl acetate/petroleum ether to afford title compound **6** as a white solid in 10% yield, silica gel TLC R_f 0.21 (ethyl acetate/*n*-hexane 50% *v/v*); m.p. 138.8 °C; δ_H (400 MHz, DMSO-d_6) 1.46 (3H, d, *J* 7.0, -CHC<u>H</u>$_3$), 3.87 (1H, q, *J* 6.9, -C<u>H</u>CH$_3$), 6.88 (1H, ddd, *J* 0.9/4.7/8.1, Ar–H), 7.01-7.04 (2H, m, 2 × Ar–H), 7.08-7.09 (1H, m, Ar–H), 7.13-7.18 (2H, m, 2 × Ar–H), 7.28 (2H, s, SO_2NH_2, exchange with D_2O), 7.33-7.41 (3H, m, 3 × Ar–H), 7.73-7.78 (4H, m, 4 x Ar–H), 10.39 (1H, s, –CONH, exchange with D_2O); δ_C (100 MHz, DMSO-d_6) 173.4 (C═O), 157.7, 157.3, 144.6, 142.9, 139.4, 131.0 (2 xAr-C), 130.9, 127.6, 124.5, 123.2, 119.8, 119.7 (3 xAr-C), 119.6, 118.4, 117.7, 46.8 (-<u>C</u>HCH$_3$), 19.5 (-CH<u>C</u>H$_3$); (ESI-HRMS): *m/z* $[M+H]^+$ calcd for $C_{21}H_{21}N_2O_4S$, 397.1217; Found, 397.1213; Elemental analysis calculated for $C_{21}H_{20}N_2O_4S$: (%) C, 63.62; H, 5.08; N, 7.07; Found, C, 63.65; H, 5.11; N, 7.05.

4.4. 2-(±)-(3-Phenoxyphenyl)-N-(4-sulfamoylphenethyl)propanamide 11

(±)-Fenoprofen (1.0 eq.), 1-ethyl-3-(3-dimethylaminopropyl)carbodiimide hydrochloride salt (EDCI. HCl, 2.0 eq.) and 1-hydroxy-7-azabenzotriazole (HOAT, 2.0 eq.), 4-(2-aminoethyl)benzenesulfonamide (2.0 eq.) and *N,N*-diisopropylethylamine (DIPEA, 4.0 eq.) in dry DMF (4.5 ml) were treated according to the general procedure previously reported in section 2.1.1. The crude product was purified via silica gel column chromatography by elution with ethyl acetate/*n*-hexane 50% *v/v* and crystallized from ethyl acetate/petroleum ether to afford title compound **11** as a white solid in 33% yield, silica gel TLC R_f 0.28 (ethyl acetate/*n*-hexane 50% *v/v*); m.p. 104.5 °C; δ_H (400 MHz, DMSO-d_6) 1.29 (3H, d, *J* 7.0, -CHC<u>H</u>$_3$), 2.71-2.75 (2H, m, –CONHCH$_2$C<u>H</u>$_2$), 3.19-3.31 (2H, m, -CONHC<u>H</u>$_2$CH$_2$), 3.56 (1H, q, *J* 7.0, -C<u>H</u>CH$_3$), 6.99-7,00 (1H, m, Ar–H), 7.01-7.07 (4H, m, 4 × Ar–H), 7.12-7.16 (1H, m, Ar–H), 7.26 (2H, s, SO_2NH_2, exchange with D_2O), 7.28-7.34 (3H, m, 3 x Ar–H), 7.37-7.42 (2H, m, 2 x Ar–H), 7.71 (2H, d, *J* 8.4, 2 x Ar–H), 8.06 (1H, t, *J* 5.6, CONH, exchange with D_2O); δ_C (100 MHz, DMSO-d_6) 173.8 (C═O), 157.5, 157.4, 145.4, 144.6, 142.9, 130.9 (2 x Ar–C), 130.7, 130.0 (2 x Ar–C), 126.5 (2 x Ar–C), 124.3, 123.3, 119.5 (2 x Ar-CH), 118.5, 117.5, 45.8 (-<u>C</u>HCH$_3$), 40.9 (-CONH<u>C</u>H$_2$CH$_2$), 35.6 (-CONHCH$_2$<u>C</u>H$_2$), 19.3 (-CH<u>C</u>H$_3$); (ESI-HRMS): *m/z* $[M+H]^+$ calcd for $C_{23}H_{25}N_2O_4S$ 425.1530; Found, 425.1524; Elemental analysis calculated for $C_{23}H_{24}N_2O_4S$: (%) C, 65.23; H, 5.47; N, 6.61; Found, C, 65.09; H, 5.56; N, 6.64.

4.5. 2-(±)-(3-Phenoxyphenyl)-N-(2-(4-sulfamoylphenoxy)ethyl) propanamide 17

(±)-Fenoprofen (1.0 eq.), 1-ethyl-3-(3-dimethylaminopropyl)carbodiimide hydrochloride salt (EDCI. HCl, 2.0 eq.) and 1-hydroxy-7-azabenzotriazole (HOAT, 2.0 eq.), 4-((3-hydroxyethyl)amino) benzenesulfonamide (2.0 eq.) and *N,N*-diisopropylethylamine (DIPEA, 4.0 eq.) in dry DMA (4.5 ml) were treated according to the general procedure previously reported in section 2.1.1. The crude product was purified via silica gel column chromatography via ethyl acetate/*n*-hexane 50% *v/v* and triturated with dichloromethane/petroleum ether to afford title compound **17** as a white solid in 13% yield, silica gel TLC R_f 0.11 (ethyl acetate/*n*-hexane 50% *v/v*); m.p. 93.1 °C; δ_H (400 MHz, DMSO-d_6) 1.34 (3H, d, *J* 7.0, -CHC<u>H</u>$_3$), 3.43-3.45 (2H, m, -CONHC<u>H</u>$_2$CH$_2$), 3.46-3.67 (1H, m, -C<u>H</u>CH$_3$), 4.07 (2H, t, *J* 5.6, –CONHCH$_2$C<u>H</u>$_2$), 6.86 (1H, ddd, *J* 0.9/2.5/8.1, Ar–H), 7.01-7.04 (3H, m, 3 × Ar–H), 7.08 (2H, d, *J* 8.9, 2 × Ar–H), 7.12 (1H, d, *J* 7.8, Ar–H), 7.15-7.19 (1H, m, Ar–H), 7.23 (2H, s, SO_2NH_2, exchange with D_2O), 7.32 (1H, t, *J* 7.9, Ar–H), 7.41 (2H, t, *J* 7.4, 2 x Ar–H), 7.76 (2H, d, *J* 8.8, 2 x Ar–H), 8.3 (1H, t, *J* 5.6, –CONH, exchange with D_2O); 174.3 (C═O), 161.7, 157.4, 157.3, 145.3, 137.3, 130.9 (2 x Ar–C), 130.7, 128.6 (2 x Ar–C), 124.3, 123.3, 119.5 (2 x Ar–C), 118.5, 117.5, 115.4 (2 x Ar–C), 67.5 (-CONHCH$_2$C<u>H</u>$_2$), 45.7 (-C<u>H</u>CH$_3$), 39.1 (-CONH<u>C</u>H$_2$CH$_2$), 19.4 (-CH<u>C</u>H$_3$); (ESI-HRMS): *m/z* $[M+H]^+$ calcd for $C_{23}H_{25}N_2O_5S$, 441,1479; Found, 441.1475; Elemental analysis calculated for $C_{23}H_{24}N_2O_5S$: (%) C, 62.71; H, 5.49; N, 6.36; Found: C, 62.75; H, 5.51; N, 6.34.

4.6. 2-(±)-(3-Phenoxyphenyl)-N-(3-(4-sulfamoylphenoxy)propyl) propanamide 24

(±)-Fenoprofen (1.0 eq.), 1-ethyl-3-(3-dimethylaminopropyl)carbodiimide hydrochloride salt (EDCI. HCl, 2.0 eq.) and 1-hydroxy-7-azabenzotriazole (HOAT, 2.0 eq.), 4-((3-hydroxy propyl)amino) benzenesulfonamide (2.0 eq.) and *N,N*-diisopropylethylamine (DIPEA, 4.0 eq.) in dry DMA (4.5 ml) were treated according to the general procedure previously reported in section 2.1.1. The crude product was triturated with DCM/petroleum ether to afford title compound **24** as a

white solid with 20% yield, silica gel TLC R_f 0.20 (ethyl acetate/*n*-hexane 50% *v/v*); m.p. 91.7 °C; δ_H (400 MHz, DMSO-d_6) 1.33 (3H, d, *J* 7.0, -CHC$\underline{H_3}$), 1.85 (2H, p, *J* 6.5, –CONHCH$_2$C$\underline{H_2}$CH$_2$), 3.17-3.24 (2H, m, -CONHC$\underline{H_2}$CH$_2$CH$_2$), 3.61 (1H, q, *J* 7.0, -C$\underline{H}$CH$_3$), 4.00 (2H, t, *J* 6.4, –CONHCH$_2$CH$_2$C$\underline{H_2}$), 6.88 (1H, ddd, *J* 0.9/2.5/8.1, Ar–H), 7.01-7.05 (5H, m, 5 x Ar–H), 7.12 (1H, d, *J* 7.8, Ar–H), 7.17 (1H, tt, *J* 1.1/7.4, Ar–H), 7.22 (2H, s, SO_2NH_2, exchange with D_2O), 7.33 (1H, d, *J* 7.9, Ar–H), 7.39-7.44 (2H, m, 2 x Ar–H), 7.76 (2H, d, *J* 8.8, 2 x Ar–H), 8.08 (1H, t, *J* 5.6, –CONH, exchange with D_2O); δ_C (100 MHz, DMSO-d_6) 174.0 (C═O), 161.9, 157.5, 157.4, 145.5, 137.0, 131.0 (2 x Ar–C), 130.7, 128.6 (2 x Ar–C), 124.3, 123.3, 119.5 (2 x Ar–C), 118.5, 117.6, 115.3 (2 x Ar–C), 66.5, 46.0 (-C$\underline{H}$CH$_3$), 36.4, 29.6, 19.4 (-CHC$\underline{H_3}$); HRMS (ESI-MS): *m/z* $[M+H]^+$ calcd for $C_{24}H_{27}N_2O_5S$, 455,1635; Found, 455.1637; Elemental analysis calculated for $C_{24}H_{26}N_2O_5S$: (%) C, 63.42; H, 5.77; N, 6.16; Found: C, 63.47; H, 5.81; N, 6.12.

4.7. Carbonic anhydrase inhibition

The CA-catalyzed CO_2 hydration activity was determined on a stopped-flow instrument (Applied Photophysics Ltd., UK). For β-CAs, bromothymol blue (0.2 mM) was used as a pH indicator, working at the absorbance maximum of 620 nm with Tris buffer (10–20 mM, pH 8.3). For hCAs, phenol red (0.2 mM) was used as a pH indicator with 20 mM HEPES buffer (pH 7.5), working at the maximum absorbance of 557 nm. Na_2SO_4 (20 mM) was added to the system to maintain a constant ionic strength. The initial rates of the CA-catalyzed CO_2 hydration reaction were followed for a period of 10–100 s. The CO_2 concentrations ranged from 1.7 to 17 mM. The enzyme concentrations ranged from 5 to 12 nM. For each compound, six traces of the initial 5–10% of the reaction were used to determine the initial velocity. Uncatalyzed reaction rates were determined in the same manner and subtracted from the total observed rates. Inhibitor stock solutions (0.1 mM) were prepared in distilled water, and dilutions up to 0.01 nM were prepared. Solutions containing the inhibitor and enzyme were preincubated for 15 min at room temperature prior to the assay to allow the formation of the enzyme–inhibitor complex. The inhibition constants (K_I) were obtained via nonlinear least-squares protocols via GraphPad Prism (v8.3.0) and the Cheng−Prusoff equation and are the means from three different measurements [34]. All the recombinant CAs were obtained in house [35–38].

4.8. Preparation of compounds and antibiotics

Lyophilized NSAIDs, CAIs and NSAID-CAIs were dissolved in DMSO (Sigma−Aldrich) prior to being added to mycobacterial cultures. Rifampicin was diluted from a ready-made solution (TOKU-E, WA, USA) to the desired concentrations prior to use. For the zebrafish infection experiment, lyophilized NSAID-CAIs were mixed with rifampicin solution and melted gelatin (Sigma−Aldrich).

4.9. Preparation of bacteria

Wild-type (wt) and bioluminescent (pMV306hsp + LuxG13 plasmid, Addgene #26161, a gift from Brian Robertson & Siouxsie Wiles) Mmr (ATCC 927) and attenuated H37Ra Mtb (ATCC 25177) were used in the experiments. The bacteria were cultured on Middlebrook 7H10 plates (Merck Millipore, MA, USA) supplemented with 10% (v/v) oleic acid dextrose catalase (BD BBL™ Middlebrook OADC Enrichment, Becton, Dickinson and Company, NJ, USA) and 0.5% (v/v) glycerol (Sigma−Aldrich) at 29 °C for one week for Mmr and at 37 °C and 5% CO_2 for three weeks for H37Ra Mtb. For planktonic cultures, bacteria were inoculated into BD Difco™ Middlebrook 7H9 broth (Becton, Dickinson and Company) supplemented with 10% (v/v) albumin dextrose catalase (BD BBL™ Middlebrook ADC Enrichment, Becton, Dickinson and Company), 0.2% (v/v) glycerol and 0.2% (v/v) Tween® 80 (Sigma−Aldrich). For biofilm medium, the broth was supplemented with only ADC, as excluding detergent allows biofilm formation [39].

4.10. Minimum duration for killing

Bioluminescent reporters were used to evaluate changes in mycobacterial drug tolerance as previously described [2]. Briefly, Mmr and H37Ra Mtb were streaked from Middlebrook 7H10 plates into planktonic or biofilm media until the OD_{600} reached 0.1. White, sterile 96-well plates (PerkinElmer, MA, USA) were filled with 192 μl of homogenous suspension, and the plates were sealed with Parafilm® M (Sigma−Aldrich). Mmr plates were cultured for seven days in the dark at 29 °C, and H37Ra Mtb plates were cultured for ten days in the dark at 37 °C and 5% CO_2. Upon initiating the assay, NSAID-CAIs and rifampicin were added on top of the bacteria to a final volume of 200 μl. Each treatment was tested in biological triplicates. To quantify luminescence, the plates were measured with a 2014 EnVision Multilabel Reader (PerkinElmer). Five horizontal and five vertical points 0.72 mm apart were measured from each well daily for four to seven days, and the results were analyzed with a Wallac EnVision Workstation 1.12 (PerkinElmer). The background signal from the medium wells was subtracted from the sample values and normalized against the untreated values at the experimental starting point. Data analysis was performed by generating time−kill curves for relative light units (RLUs) to time in GraphPad Prism (v8.3.0). Areas under the curves (AUCs) were calculated from time−kill curves 24 to 96 h post-exposure. Statistical significance was calculated between the AUCs via one-way ANOVA and Dunnett's multiple comparisons test or two-way ANOVA and Tukey's post hoc test in GraphPad Prism (v8.3.0).

To quantify changes in colony-forming units (CFUs), bioluminescent Mmr biofilms were prepared, NSAID-CAIs and rifampicin were added, and luminescence was measured as described for the bioluminescent MDK assay. The cultures were transferred into clear U-shaped Nunc™ 96-well plates (Thermo Fisher Scientific) daily from 0 to 96 h post-exposure. The bacteria were pelleted at 800 × g for 10 min and resuspended in BD Difco™ Middlebrook 7H9 medium supplemented with 0.5% (v/v) Tween® 80 (100 μl). The plates were incubated on a shaker (150 rpm) in the dark for 2 h at 29 °C before a 10-fold dilution series was made in 1x phosphate-buffered saline (PBS, pH 7.4) (Medicago AB, Sweden) with 0.5% (v/v) Tween® 80. A dilution series of three parallel samples was plated onto Middlebrook 7H10 plates in triplicate. The CFUs were counted after six days at 29 °C. The values were corrected with the dilution factor, and the statistical significance of the time−kill curve AUCs was calculated via one-way ANOVA and Dunnett's post hoc test in GraphPad Prism (v8.3.0).

4.11. Minimum inhibitory concentration

A minimum inhibitory concentration (MIC) assay, modified from Hall et al. [40], was used to assess the growth-inhibiting effects of NSAID-CAIs on both Mmr and H37Ra Mtb. Briefly, the bacteria were streaked into sterile 1x PBS (pH 7.4) with 0.2% (v/v) Tween® 80 until the OD_{600} reached 0.1. The top 200 μl of the suspension was mixed with 11 ml of medium and further distributed (100 μl/well) on sterile, clear Nunc™ 96-well plates (Thermo Fisher Scientific). NSAID-CAIs were resuspended in medium and added on top of the bacteria to a total volume of 200 μl. The control inoculums were streaked on Middlebrook 7H10 plates to quantify CFUs. Mmr plates were cultured for six days in the dark at 29 °C, and H37Ra Mtb plates were cultured for 14 days in the dark at 37 °C and 5% CO_2. Final turbidity changes were measured with a 2014 Envision Multilabel Reader. The OD_{600} was measured at twelve points per well, and values from the medium wells were subtracted from the values of the treated samples. MIC 50% (MIC_{50}) values were calculated from the trend lines of the OD_{600} to concentration curves.

4.12. Maintenance of zebrafish and ethical statement

Wild-type AB line adult zebrafish were maintained at 28.5 °C under standard conditions. Prior to infection, adult zebrafish were transferred from flow-through tanks (Aquatic Habitats, FL, USA) to a flow-through system (Aqua Schwarz GmbH, Germany) in a separate laboratory. For toxicity evaluation, embryos were bred and collected as described previously [41]. Briefly, at 1 to 2 h post-fertilization, the embryos were collected via a sieve, rinsed with embryonic medium [5.0 mM NaCl, 0.17 mM KCl, 0.33 mM $CaCl_2$, 0.33 mM $MgSO_4$, and 0.1% w/v methylene blue (Sigma–Aldrich)] and raised overnight at 28.5 °C. All the fish experiments were performed at the zebrafish facility of Tampere University. The research was authorized by the National Animal Experiment Board (ESAVI/10079/04.10.06/2015). Animal experiment permits (ESAVI/17803/2019 and ESAVI/14286/2022) were granted by the Animal Experiment Board of the Regional State Administrative Agency of Southern Finland. All zebrafish experiments were carried out in accordance with the Finnish Act on the Protection of Animals Used for Scientific or Educational Purposes (497/2013) and the EU Directive on the Protection of Animals Used for Scientific Purposes (2010/63/EU). Care was taken to ameliorate suffering by anesthetizing or euthanizing the zebrafish with 3-amino benzoic acid ethyl ester (tricaine, Sigma–Aldrich). The fish were euthanized upon meeting any of the humane endpoint criteria, such as abnormal swimming behavior, gasping, swelling or infectious skin ulcers.

4.13. Determination of the LC_{50} and toxic phenotypes

Prior to treating adult zebrafish with NSAID-CAIs, toxicity evaluation was performed in a larval model as described previously [41]. Twenty healthy embryos at 1 day post-fertilization (dpf) per group were chosen randomly, and the embryos were raised in embryonic medium supplemented with NSAID-CAIs in 1.6% v/v DMSO in clear 24-well plates (VWR® International, PA, USA). Mortality was recorded daily until 5 dpf, when the final resulting phenotype was also assessed. The phenotypes were evaluated according to eight parameters: mortality, hatching, presence of edema, swimming activity, yolk sack consumption, active heartbeat, body shape and swim bladder development. Representative larvae were embedded in 1.7% methylcellulose (Sigma–Aldrich) and imaged with a digital camera (Axiocam 105, Carl Zeiss, Germany) attached to a stereomicroscope (Stemi 2000-C, Carl Zeiss). Dose–response curves were generated with GraphPad Prism (v8.3.0) to evaluate the lethal concentration 50% (LC_{50}) values. Phenotype images were analyzed with ZEN 2.3 Lite (Carl Zeiss).

4.14. Adult zebrafish infections

For adult zebrafish infections, the Mmr inoculum was cultured in 10 ml of planktonic medium in the dark at 29 °C. After three days, the culture was diluted to an OD_{600} of 0.08 and cultured to the logarithmic growth stage. The top 1 ml was pelleted at 10,000 × g for 3 min and resuspended in 1x PBS with 0.3 mg/ml phenol red (Sigma–Aldrich) as a tracer. The zebrafish were infected intrachoelomically with 56 ± 12 CFUs of Mmr in the abdominal cavity via a 30 G Omnican® 100 insulin needle (B. Braun AG, Germany), as previously described [23]. Infection doses were verified by plating onto Middlebrook 7H10 plates every 15 min. The CFUs were counted after six days in the dark at 29 °C. The zebrafish were allowed to recover in system water and placed randomly back in tanks at a density of 15–20 zebrafish per tank. Treatments were assigned per tank. Welfare was assessed daily, and individuals with any symptoms were euthanized with a tricaine overdose. The fish were raised according to standard protocols until 4 weeks post-infection (wpi), when treatment was initiated [23]. NSAID-CAIs, rifampicin, and gelatin (Sigma–Aldrich) were manually powderized into Gemma Micro 500 fish food (Skretting, Norway). The daily oral doses used were 32 mg/kg rifampicin and 68 mg/kg compound **12** per fish or 32 mg/kg rifampicin and 70 mg/kg compound **19** per fish.

At 4, 6, 8, and 10 wpi, individual bacterial burdens were quantified from the internal organs of the zebrafish. Briefly, the fish were euthanized, and internal organ blocks were collected in homogenization tubes (Omni International, GA, USA) with 100 µl of 1x PBS (pH 7.4) and six ceramic beads (⌀ 2.8 mm, Omni International). By keeping the samples on ice, 300 µl of 6.66% sodium dodecyl sulfate (Sigma–Aldrich) in 1x PBS was added, and the samples were homogenized twice on dry ice for 40 s at 6.5 s/m with a CoolPrep™ System (MP Biomedicals LCC, CA, USA). The homogenates and a 1:1 volume of MycoPrep™ Reagent (BD BBL™ MycoPrep™ Mycobacterial System Digestion/Decontamination Kit) were incubated for 15 min with occasional gentle shaking. The digestion mixture was deactivated with MycoPrep™ Phosphate Buffer, and the samples were centrifuged for 20 min at 3000 × g. The pellets were resuspended in 1x PBS to a final volume of 500 µl, and 10-fold dilution series were plated on Middlebrook 7H10 plates in triplicate. The CFUs were counted after six days at 29 °C. The values were corrected with the dilution factor, and significant differences between treatment groups at each time point were calculated with Mann–Whitney tests in GraphPad Prism (v8.3.0).

4.15. Statistics

MDK-assays utilized one-way ANOVA and Dunnett's post hoc tests to test for statistical significance as the bacterial population was assumed to be normally distributed and each treatment was compared against a control treatment. Similarly, two-way ANOVA and Tukey's post hoc test was used to test for statistical significance in MDK-assays comparing multiple treatments against each other. Statistical significance of bacterial burden within adult zebrafish was assessed with non-parametric Mann-Whitney U-tests as bacterial burden has high variability between individuals and the datasets are not normally distributed (Shapiro-Wilk).

CRediT authorship contribution statement

Jenny Parkkinen: Data curation, Formal analysis, Funding acquisition, Investigation, Visualization, Writing – original draft, Writing – review & editing. **Özlem Akgul:** Data curation, Investigation, Methodology. **Emanuela Berrino:** Formal analysis, Methodology. **Fabrizio Carta:** Conceptualization, Data curation, Funding acquisition, Investigation, Project administration, Resources, Supervision, Validation, Visualization, Writing – original draft, Writing – review & editing. **Silvia Selleri:** Data curation, Methodology, Validation. **Milka Hammarén:** Methodology, Supervision. **Ashok Aspatwar:** Conceptualization, Methodology, Supervision. **Gianluca Bartolucci:** Data curation, Methodology. **Clemente Capasso:** Data curation, Methodology. **Mataleena Parikka:** Conceptualization, Funding acquisition, Methodology, Project administration, Resources, Supervision, Writing – review & editing. **Seppo Parkkila:** Conceptualization, Funding acquisition, Project administration, Resources, Supervision, Writing – review & editing. **Claudiu T. Supuran:** Conceptualization, Funding acquisition, Project administration, Resources, Supervision, Validation.

Declaration of competing interest

The authors declare the following financial interests/personal relationships which may be considered as potential competing interests: Milka Hammarén has patent pending to Tampere University. Milka Hammarén is an inventor of a patent for a method used in this paper and is leading a project looking into the commercial value of the method and the findings. Mataleena Parikka has patent pending to Tampere University. The patent is on a screening method described in this article. If there are other authors, they declare that they have no known competing financial interests or personal relationships that could have appeared to influence the work reported in this paper.

Acknowledgments

We thank Sanna Kavén, Rosa Korhonen, Saara Lehmusvaara, Leena Mäkinen, Maarit Patrikainen and Hannaleena Piippo for assistance with the laboratory experiments. We also thank the Tampere Zebrafish Core Facility, which is partly funded by Biocenter Finland, for maintaining and providing the zebrafish. We thank Harlan Barker for language editing.

This study was funded by Foundation of the Finnish Anti-Tuberculosis Association (JP), Jane & Aatos Erkko Foundation (MP, SP), Orion Research Foundation (JP), the Paulo Foundation (JP), Research Council of Finland (MP, SP, MH), Sigrid Juselius Foundation (MP), Tampere Tuberculosis Foundation (AA, JP, MP, SP) and Väinö ja Laina Kiven Säätiö (JP).

Appendix A. Supplementary data

Supplementary data to this article can be found online at https://doi.org/10.1016/j.ejmech.2026.119037.

Data availability

No data was used for the research described in the article.

References

[1] World Health Organization, Global Tuberculosis Report 2024, 2024. ISBN 978-92-4-010154-8.
[2] K. Savijoki, H. Myllymäki, H. Luukinen, L. Paulamäki, L.M. Vanha-Aho, et al., Surface-shaving proteomics of Mycobacterium marinum identifies biofilm subtype-specific changes affecting virulence, tolerance, and persistence, mSystems 6 (3) (2021) 10–1128, https://doi.org/10.1128/mSystems.00500-21.
[3] A.K. Ojha, A.D. Baughn, D. Sambandan, T. Hsu, X. Trivelli, et al., Growth of Mycobacterium tuberculosis biofilms containing free mycolic acids and harbouring drug-tolerant bacteria, Mol. Microbiol. 69 (1) (2008) 164–174, https://doi.org/10.1111/j.1365-2958.2008.06274.x.
[4] K. Dheda, T. Gumbo, G. Maartens, K.E. Dooley, R. McNerney, et al., The epidemiology, pathogenesis, transmission, diagnosis, and management of multidrug-resistant, extensively drug-resistant, and incurable tuberculosis, Lancet Respir. Med. 5 (4) (2017) 291–360, https://doi.org/10.1016/S2213-2600(17)30079-6.
[5] C.C. Leung, C.M. Tam, S.L. Chan, M. Chan-Yeung, C.K. Chan, et al., Efficacy of the BCG revaccination programme in a cohort given BCG vaccination at birth in Hong Kong, Int. J. Tuberc. Lung Dis 5 (8) (2001) 717–723.
[6] F. Ma, H. Zhou, Z. Yang, C. Wang, Y. An, et al., Gene expression profile analysis and target gene discovery of Mycobacterium tuberculosis biofilm, Appl. Microbiol. Biotechnol. 105 (12) (2021) 5123–5134, https://doi.org/10.1007/s00253-021-11361-4.
[7] P. Chakraborty, S. Bajeli, D. Kaushal, B.D. Radotra, A. Kumar, Biofilm formation in the lung contributes to virulence and drug tolerance of Mycobacterium tuberculosis, Nat. Commun. 12 (1) (2021) 1606, https://doi.org/10.1038/s41467-021-21748-6.
[8] S.H. Kaufmann, A. Dorhoi, R.S. Hotchkiss, R. Bartenschlager, Host-directed therapies for bacterial and viral infections, Nat. Rev. Drug Discov. 17 (1) (2018) 35–56, https://doi.org/10.1038/nrd.2017.162.
[9] A. Zumla, M. Maeurer, Host-Directed Therapies Network (Hdt-Net) Consortium (2015). Host-directed therapies for tackling multi-drug resistant tuberculosis: learning from the pasteur-bechamp debates, Clin. Infect. Dis. 61 (9) (2015) 1432–1438, https://doi.org/10.1093/cid/civ631.
[10] T.R. Hawn, A.I. Matheson, S.N. Maley, O. Vandal, Host-directed therapeutics for tuberculosis: can we harness the host? Microbiol. Mol. Biol. Rev. 77 (4) (2013) 608–627, https://doi.org/10.1128/mmbr.00032-13.
[11] D. Kiran, B.K. Podell, M. Chambers, R.J. Basaraba, Host-directed therapy targeting the Mycobacterium tuberculosis granuloma: a review, in: Seminars in Immunopathology, vol. 38, Springer Berlin Heidelberg, Berlin/Heidelberg, 2016, March, pp. 167–183, https://doi.org/10.1007/s00281-015-0537-x, 2.
[12] V.M. Kroesen, M.I. Gröschel, N. Martinson, A. Zumla, M. Maeurer, et al., Non-steroidal anti-inflammatory drugs as host-directed therapy for tuberculosis: a systematic review, Front. Immunol. 8 (2017) 772, https://doi.org/10.3389/fimmu.2017.00772.
[13] L. Lucarini, M. Durante, S. Sgambellone, C. Lanzi, E. Bigagli, et al., Effects of new NSAID-CAI hybrid compounds in inflammation and lung fibrosis, Biomolecules 10 (9) (2020) 1307, https://doi.org/10.3390/biom10091307.
[14] L. Micheli, M. Bozdag, O. Akgul, F. Carta, C. Guccione, et al., Pain relieving effect of-NSAIDs-CAIs hybrid molecules: systemic and intra-articular treatments against rheumatoid arthritis, Int. J. Mol. Sci. 20 (8) (2019) 1923, https://doi.org/10.3390/ijms20081923.
[15] O. Akgul, L. Di Cesare Mannelli, D. Vullo, A. Angeli, C. Ghelardini, et al., Discovery of novel nonsteroidal anti-inflammatory drugs and carbonic anhydrase inhibitors hybrids (NSAIDs–CAIs) for the management of rheumatoid arthritis, J. Med. Chem. 61 (11) (2018) 4961–4977, https://doi.org/10.1021/acs.jmedchem.8b00420.
[16] S. Bua, L. Lucarini, L. Micheli, M. Menicatti, G. Bartolucci, et al., Bioisosteric development of multitarget nonsteroidal anti-inflammatory drug–carbonic anhydrases inhibitor hybrids for the management of rheumatoid arthritis, J. Med. Chem. 63 (5) (2019) 2325–2342, https://doi.org/10.1021/acs.jmedchem.9b01130.
[17] S. Bua, L. Di Cesare Mannelli, D. Vullo, C. Ghelardini, G. Bartolucci, et al., Design and synthesis of novel nonsteroidal anti-inflammatory drugs and carbonic anhydrase inhibitors hybrids (NSAIDs–CAIs) for the treatment of rheumatoid arthritis, J. Med. Chem. 60 (3) (2017) 1159–1170.
[18] F. Margheri, M. Ceruso, F. Carta, A. Laurenzana, L. Maggi, et al., Overexpression of the transmembrane carbonic anhydrase isoforms IX and XII in the inflamed synovium, J. Enzyme Inhib. Med. Chem. 31 (sup4) (2016) 60–63, https://doi.org/10.1080/14756366.2016.1217857.
[19] S.J. Rose, L.E. Bermudez, Identification of bicarbonate as a trigger and genes involved with extracellular DNA export in mycobacterial biofilms, mBio 7 (6) (2016) 10–1128, https://doi.org/10.1128/mbio.01597-16.
[20] A.S. Covarrubias, A.M. Larsson, M. Högbom, J. Lindberg, T. Bergfors, et al., Structure and function of carbonic anhydrases from Mycobacterium tuberculosis, J. Biol. Chem. 280 (19) (2005) 18782–18789, https://doi.org/10.1074/jbc.M414348200.
[21] F. Carta, A. Maresca, A.S. Covarrubias, S.L. Mowbray, T.A. Jones, et al., Carbonic anhydrase inhibitors. Characterization and inhibition studies of the most active β-carbonic anhydrase from Mycobacterium tuberculosis, Rv3588c, Bioorg. Med. Chem. Lett. 19 (23) (2009) 6649–6654, https://doi.org/10.1016/j.bmcl.2009.10.009.
[22] I. Nishimori, T. Minakuchi, D. Vullo, A. Scozzafava, A. Innocenti, et al., Carbonic anhydrase inhibitors. Cloning, characterization, and inhibition studies of a new β-carbonic anhydrase from Mycobacterium tuberculosis, J. Med. Chem. 52 (9) (2009) 3116–3120, https://doi.org/10.1021/jm9003126.
[23] H. Luukinen, M.M. Hammarén, L.M. Vanha-Aho, M. Parikka, Modeling tuberculosis in Mycobacterium marinum infected adult zebrafish, JoVE J. (140) (2018) 58299, https://doi.org/10.3791/58299.
[24] M. Parikka, M.M. Hammaren, S.K.E. Harjula, N.J. Halfpenny, K.E. Oksanen, et al., Mycobacterium marinum causes a latent infection that can be reactivated by gamma irradiation in adult zebrafish, PLoS Pathog. 8 (9) (2012) e1002944, https://doi.org/10.1371/journal.ppat.1002944.
[25] R.G. Khalifah, The carbon dioxide hydration activity of carbonic anhydrase: I. Stop-flow kinetic studies on the native human isoenzymes B and C, J. Biol. Chem. 246 (8) (1971) 2561–2573, https://doi.org/10.1016/S0021-9258(18)62326-9.
[26] A. Manaithiya, R. Bhowmik, K. Bhattacharya, R. Ray, S.S. Shyamal, et al., A cheminformatics and network pharmacology approach to elucidate the mechanism of action of Mycobacterium tuberculosis γ-carbonic anhydrase inhibitors, Front. Pharmacol. 15 (2024) 1457012, https://doi.org/10.3389/fphar.2024.1457012.
[27] A. Brauner, O. Fridman, O. Gefen, N.Q. Balaban, Distinguishing between resistance, tolerance and persistence to antibiotic treatment, Nat. Rev. Microbiol. 14 (5) (2016) 320–330, https://doi.org/10.1038/nrmicro.2016.34.
[28] S. Vijay, H.N. Nhung, N.L.H. Bao, D.D.A. Thu, L.P.T. Trieu, et al., Most-probable-number-based minimum duration of killing assay for determining the spectrum of rifampicin susceptibility in clinical Mycobacterium tuberculosis isolates, Antimicrob. Agents Chemother. 65 (3) (2021) 10–1128, https://doi.org/10.1128/AAC.01439-20.
[29] C.M. Sassetti, E.J. Rubin, Genetic requirements for mycobacterial survival during infection, Proc. Natl. Acad. Sci. USA 100 (22) (2003) 12989–12994, https://doi.org/10.1073/pnas.2134250100.
[30] S.J. Dechow, R. Goyal, B.K. Johnson, E.R. Haiderer, R.B. Abramovitch, Carbon dioxide regulates Mycobacterium tuberculosis PhoPR signaling and virulence, Infect. Immun. 93 (3) (2025) e00568, https://doi.org/10.1128/iai.00568-24, 24.
[31] G. Degiacomi, B. Gianibbi, D. Recchia, G. Stelitano, G.I. Truglio, et al., CanB, a druggable cellular target in Mycobacterium tuberculosis, ACS Omega 8 (28) (2023) 25209–25220, https://doi.org/10.1021/acsomega.3c02311.
[32] B. Puig-Collderram, S. Domene-Ochoa, M. Salvà-Comas, M.M. Montero, X. Duran, et al., ATP bioluminescence assay to evaluate antibiotic combinations against extensively drug-resistant (XDR) Pseudomonas aeruginosa, Microbiol. Spectr. 10 (4) (2022) e00651, https://doi.org/10.1128/spectrum.00651-22, 22.
[33] J.P. Dalton, B. Uy, K.S. Okuda, C.J. Hall, W.A. Denny, et al., Screening of anti-mycobacterial compounds in a naturally infected zebrafish larvae model, J. Antimicrob. Chemother. 72 (2) (2017) 421–427, https://doi.org/10.1093/jac/dkw421.
[34] A.A. Lebedev, P. Young, M.N. Isupov, O.V. Moroz, A.A. Vagin, et al., JLigand: a graphical tool for the CCP4 template-restraint library, Acta Crystallogr. D Biol. Crystallogr. 68 (4) (2012) 431–440, https://doi.org/10.1107/S090744491200251X.
[35] J.Y. Winum, F. Carta, C. Ward, P. Mullen, D. Harrison, et al., Ureido-substituted sulfamates show potent carbonic anhydrase IX inhibitory and antiproliferative activities against breast cancer cell lines, Bioorg. Med. Chem. Lett. 22 (14) (2012) 4681–4685, https://doi.org/10.1016/j.bmcl.2012.05.083.
[36] M.Y. Mboge, B.P. Mahon, N. Lamas, L. Socorro, F. Carta, et al., Structure activity study of carbonic anhydrase IX: selective inhibition with ureido-substituted benzenesulfonamides, Eur. J. Med. Chem. 132 (2017) 184–191, https://doi.org/10.1016/j.ejmech.2017.03.026.

[37] F. Carta, D. Vullo, A. Maresca, A. Scozzafava, C.T. Supuran, New chemotypes acting as isozyme-selective carbonic anhydrase inhibitors with low affinity for the offtarget cytosolic isoform II, Bioorg. Med. Chem. Lett. 22 (6) (2012) 2182–2185, https://doi.org/10.1016/j.bmcl.2012.01.129.

[38] M. Abdoli, A. Angeli, M. Bozdag, F. Carta, A. Kakanejadifard, et al., Synthesis and carbonic anhydrase I, II, VII, and IX inhibition studies with a series of benzo [d] thiazole-5-and 6-sulfonamides, J. Enzyme Inhib. Med. Chem. 32 (1) (2017) 1071–1078, https://doi.org/10.1080/14756366.2017.1356295.

[39] R.J. Basaraba, A.K. Ojha, Mycobacterial biofilms: revisiting tuberculosis Bacilli in extra-cellular necrotizing lesions, Microbiol. Spectr. 5 (3) (2017), https://doi.org/10.1128/microbiolspec.TBTB2-0024-2016, 5.3.15.

[40] L. Hall, K.P. Jude, S.L. Clark, N.L. Wengenack, Antimicrobial susceptibility testing of Mycobacterium tuberculosis complex for first and second line drugs by broth dilution in a microtiter plate format, JoVE J. (52) (2011) 3094, https://doi.org/10.3791/3094.

[41] A. Aspatwar, M.M. Hammaren, M. Parikka, S. Parkkila, Rapid evaluation of toxicity of chemical compounds using zebrafish embryos, JoVE J. (2019) 1–7, https://doi.org/10.3791/59315, 2019.